Nuclear Instruments and Methods in Physics Research A 624 (2010) 656–661

Contents lists available at ScienceDirect

Nuclear Instruments and Methods in Physics Research A

journal homepage: www.elsevier.com/locate/nima

Fabrication and spectroscopy results of mercuric iodide Frisch collar detectors

E. Ariesanti [a,*], A. Kargar [b], D.S. McGregor [a]

[a] SMART Laboratory, Department of Mechanical and Nuclear Engineering, Kansas State University, Manhattan, KS 66506, USA
[b] Radiation Monitoring Devices, Inc., 44 Hunt Street, Watertown, MA 02472, USA

ARTICLE INFO

Article history:
Received 21 July 2010
Received in revised form
15 September 2010
Accepted 20 September 2010
Available online 29 September 2010

Keywords:
Mercuric iodide
Vapor growth
Horizontal furnace
Polyethylene
Frisch collar spectrometer

ABSTRACT

A tetragonal prismatic HgI_2 crystal grown with low molecular weight ($\overline{M}_w$) polyethylene addition in a horizontal furnace has been fabricated into a $2.1 \times 2.1 \times 4.1\ mm^3$ Frisch collar spectrometer. With no electronic correction nor LN_2 cooling, an energy resolution of 1.8% FWHM at 662 keV (^{137}Cs) is achieved. Spectra from ^{241}Am (4.7% FWHM at 59.5 keV), ^{57}Co (4.0% FWHM at 122 keV), ^{133}Ba (4.4% FWHM at 80 keV and 2.5% FWHM at 356 keV), ^{198}Au (2.6% FWHM at 411 keV), and ^{60}Co (1.2% FWHM at 1173 keV) are also reported.

1. Introduction

Mercuric iodide (HgI_2) is considered a candidate material for room-temperature γ-ray detectors mainly due to its high atomic numbers ($Z_{Hg}=80$, $Z_I=53$) and wide band gap (~2.13 eV). Despite these favorable attributes, HgI_2 suffers from several drawbacks, such as low hole mobility [1], low yield strength [2], and polarization [3]. These drawbacks unfortunately have prevented a wider use of HgI_2 single crystals as room temperature γ-ray detectors. Due to their low mobility, holes are trapped more easily than electrons. Unfortunately the influence of trapped charges is compromised and their contribution to charge induction diminished. Because a large deviation in charge carrier collection translates into poor energy resolution, removal of the hole contribution from the charge induction process and/or the reduction of hole carrier traps will improve energy resolution.

One detector design that precludes much of the hole contribution to charge induction is the Frisch collar detector design [4–7]. With the Frisch collar design the weighting potential of the device can be altered such that the contribution of the hole motion towards charge induction is significantly reduced. The simplest Frisch collar detector utilizes a tetragonal prismatic crystal with an aspect ratio (the ratio of length to width) of two [8]. Therefore, ordinarily a bulk crystal must be cut into the proper shape. However, cutting a HgI_2 crystal into such a shape risks damaging the crystal due to the low yield strength of the material [2]. Moreover, the subsequent polishing of the crystal may introduce additional impurities and crystal defects.

Impurities can also be incorporated through the pre-growth and crystallization processes. Choosing the appropriate growth method can also reduce impurities and diminish the effects of crystal dislocations. Prismatic HgI_2 crystals have been grown by solution or solvent methods [9,10]. It was noticed, however, that solution or solvent molecules were included in the solids, which constitute impurities in the crystals. Another growth method, growth by melt, cannot be employed due to the irreversible phase transformation near 130 °C. Vapor growth is therefore a more suitable method for growing HgI_2, which is also known for its appreciable vapor pressure at room temperature. The most common methods of growing HgI_2 by the vapor are the bulk crystal growth in a vertical furnace and the polyethylene-aided crystal growth in a horizontal furnace.

The vertical furnace method, developed at EG&G Santa Barbara [11–13], is based on the modified Scholz method [14]. This method was used to routinely grow HgI_2 crystals between 100 and 200 g within 1–2 months. Although much of the material is harvested at the end of the growth period, not all parts of the grown crystal are suitable for detector fabrication. Therefore, extensive cutting and etching must be done to shape and prepare the surfaces of the crystals. As mentioned previously, these post-growth processes predispose HgI_2 to inclusion of extrinsic impurities and plastic deformation. Therefore extensive post-growth processes pose harm to the integrity of the crystals. Previous attempts to cut and fabricate HgI_2 into Frisch collar detectors demonstrated only limited success [15].

Another vapor growth method for HgI_2 production is the horizontal growth method that was first introduced by Faile in 1980 [16]. The quality (i.e., purity) of the HgI_2 starting material has a huge effect on the habit of the grown crystals. It was shown

* Corresponding author. Tel.: +1 785 532 6128; fax: +1 785 532 7057.
E-mail address: ancilla@k-state.edu (E. Ariesanti).

0168-9002/$ - see front matter © 2010 Elsevier B.V. All rights reserved.
doi:10.1016/j.nima.2010.09.075

in previous work that growth with unpurified HgI_2 yields platelet shaped crystals [16–18], while prismatic tetragonal crystals can be grown with *purified* HgI_2. The prismatic HgI_2 crystals have the correct shape for Frisch collar detectors. Unlike the HgI_2 vapor growth in a vertical furnace, however, HgI_2 growth with the Faile method has not been fully understood. In the past, efforts to determine the causes for this habit modification focused on the effect of the added polymer on mass transport, purification, and HgI_2 stoichiometry [17,18,19,20]. To date, however, none of these efforts has satisfactorily explained the effect of polymer addition in modifying the HgI_2 crystal habit.

The objectives of the HgI_2 research in the SMART Laboratory at Kansas State University are: (1) to observe and determine the effects of polymer addition on crystal morphology, (2) to grow square prismatic crystals of good quality for Frisch collar detectors, and (3) to characterize HgI_2 crystals and Frisch collar detectors. This work summarizes the HgI_2 Frisch collar detector fabrication and analyzes the spectrometric capability of the detectors. A full summary on the HgI_2 growth by the Faile method along with a description on the effects of polymer (specifically polyethylene) on the change of morphology in crystals is described elsewhere.

2. Theoretical considerations

2.1. HgI_2 material properties

Several crystal structures of HgI_2 have been observed [21,22], with α-HgI^2 as the most stable structure at ambient temperatures. The space group designation for α-HgI^2 is $P4_2/nmc$ [23], for a tetragonal crystal structure with crystal parameters $a=b=4.316$ Å and $c=12.450$ Å. It has a layered structure, with the adjacent layers stacked along the [0 0 1] axis being held by weak van der Waals bonds.

Because of the anisotropy in crystal parameters, the electronic and other physical properties of α-HgI_2 are expected to be direction-dependent. For example, $\mu_{e,h,[0\,0\,1]}$ are not necessarily the same as $\mu_{e,h,\perp[0\,0\,1]}$. To date, however, only $\mu_{e,h,[0\,0\,1]}$ have been measured [1], with $\mu_{h,[0\,0\,1]}$ about one order of magnitude smaller than $\mu_{e,[0\,0\,1]}$.

2.2. Induced charge

Suppose a γ-ray undergoes an interaction at position $\vec{r}$ and a number of electron–hole pairs (for a total of initial charge Q_0) are created. Due to the presence of the electric field, these charges move towards their respective electrodes. As these charges are moving, an induced current due to the motion of these charges can be monitored at a chosen conductor (in this case, at the anode). The induced current can be determined by using the concept of the weighting potential, which is derived from first principles using Green's second identity (i.e., *Green's theorem*) [24]. Integrating the induced current produces the induced charge measured from the radiation event. The weighting potential concept has been used by Shockley [25] and Ramo [26] to solve the induced current due to a moving charge in a vacuum tube. The concept has also been used to determine the induced charge in semiconductor detectors [4,27–29].

According to Ramo's theorem [26] the induced current due to a charge Q_0 moving at velocity $\vec{v}(\vec{r})$ is

$$I(\vec{r}) = Q_0\vec{E}_w(\vec{r})\cdot\vec{v}(\vec{r}) = Q_0|\vec{E}_w(\vec{r})||\vec{v}(\vec{r})|\cos\theta \quad (1)$$

where $\vec{E}_w(\vec{r})$ is the weighting field. In differential terms, Eq. (1) can be written as

$$\frac{dQ(\vec{r})}{dt} = -Q_0|\nabla V_w(\vec{r})|\left|\frac{d\vec{r}}{dt}\right|\cos\theta \quad (2)$$

where $I(\vec{r}) \equiv dQ(\vec{r})/dt$ and $V_w(\vec{r})$ is the weighting potential. The weighting potential $V_w(\vec{r})$ can be defined simply as the actual potential at $\vec{r}$, $V(\vec{r})$, in a medium with no stationary charges or $\rho=0$, *normalized* to the potential at the collecting or monitoring contact [30].

2.2.1. Planar detector

Due to the tetragonal prismatic shape of the HgI_2 device, the physics of the HgI_2 planar device can be explained with Cartesian coordinates in one dimension (1D). Fig. 1 shows the length-wise cross-section of a planar detector of length L and side h. The planar detector can be represented as a parallel plate capacitor bounding a semiconducting material with a dielectric constant κ. One of the plates, designated as the cathode, is grounded $V_{cathode}=0$. The second plate, the anode, is held at a positive bias ($V_{anode}=V_a>0$). For a two-terminal device, the electric and weighting field vectors are in the same direction [31]. Because a charged particle moves along an electric field line, $\cos\theta$ is equal to either 1 or -1 depending on the type of the charge particle and the direction of the electric field. Assuming that the particle is moving *in the direction* of the electric field, Eq. (1) can be written as

$$I(\vec{r}) = Q_0|\vec{E}_w(\vec{r})|\,|\vec{v}(\vec{r})|. \quad (3)$$

In differential terms and for a 1D case, Eq. (3) becomes (the vector notation for x is dropped for simplification)

$$\frac{dQ(x)}{dt} = -Q_0\frac{dV_w(x)}{dx}\frac{dx}{dt}. \quad (4)$$

Eq. (4) can be approximated as

$$\frac{\Delta Q(x)}{\Delta t} \approx -Q_0\frac{\Delta V_w(x)}{\Delta x}\frac{\Delta x}{\Delta t} \quad (5)$$

which when simplified further yields

$$\Delta Q(x) \approx -Q_0\Delta V_w(x). \quad (6)$$

Eq. (6) shows that the change in induced charge is proportional to the change in the weighting potential. To account for charge carrier trapping in the material, a factor $\exp(-\Delta t/\tau)$ is multiplied to the initial charge Q_0, thus, Eq. (6) becomes

$$\Delta Q(x) \approx -Q_0\exp\left(-\frac{\Delta t}{\tau}\right)\Delta V_w(x) = -Q_0\exp\left(-\frac{\Delta x}{|v(x)|\tau}\right)\Delta V_w(x)$$

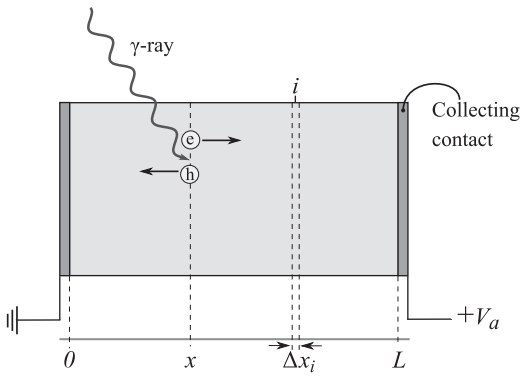

Fig. 1. Planar device configuration.

$$= -Q_0 \exp\left(-\frac{\Delta x}{\mu\tau|\vec{E}(x)|}\right)\Delta V_w(x)$$
$$= -Q_0 \exp\left(-\frac{\Delta x}{\mu\tau|\vec{E}(x)|}\right)|\vec{E}_w(x)|\Delta x \quad (7)$$

where Δx is the incremental distance traveled by a charge carrier (see Fig. 1). The *total* induced charge due to interaction at x, $Q(x)$, is

$$Q(x) = Q_e(x) + Q_h(x) = Q_0\left[\sum_i |\vec{E}_w(x_i)| \exp\left(-\frac{\Delta x_{e,i}}{\mu_e\tau_e|\vec{E}(x_i)|}\right)\Delta x_{e,i}.\right.$$
$$\left. + \sum_i |\vec{E}_w(x_i)| \exp\left(-\frac{\Delta x_{h,i}}{\mu_h\tau_h|\vec{E}(x_i)|}\right)\Delta x_{h,i}\right] \quad (8)$$

where $\Delta x_{e,i}$ and $\Delta x_{h,i}$ are the incremental distances traveled by electrons and holes, respectively, and $\vec{E}(x_i)$ is the electric field at x_i (see Fig. 1). For a planar detector configuration the weighting potential, $|\vec{E}_w(x)| = 1/L$, is obtained by solving the Laplace equation and is a constant. The electric field $\vec{E}(x)$ is obtained by solving the Poisson equation. For a planar detector configuration with a grounded cathode and an anode biased at $V_a = V(L)$, the electric field is $|\vec{E}(x)| = V(L)/L$, which is a constant. Eq. (8) can be written as integrals as shown in Eq. (9) for a planar device

$$Q(x) = Q_0|\vec{E}_w(x)|\left[\int_x^L \exp\left(-\frac{L-x'}{\mu_e\tau_e|\vec{E}(x)|}\right)dx'\right.$$
$$\left. + \int_x^0 \exp\left(-\frac{x'}{\mu_h\tau_h|\vec{E}(x)|}\right)dx'\right]. \quad (9)$$

The solution to Eq. (9) is

$$Q(x) = Q_0|\vec{E}_w(\vec{x})|\left[\mu_e\tau_e|\vec{E}(x)|\left(1-\exp\left(-\frac{L-x}{\mu_e\tau_e|E(x)|}\right)\right)\right.$$
$$\left. + \mu_h\tau_h|\vec{E}(x)|\left(1-\exp\left(-\frac{x}{\mu_h\tau_h|\vec{E}(x)|}\right)\right)\right]. \quad (10)$$

Substituting for $|\vec{E}_w(x)|$ and $|\vec{E}(x)|$, the Hecht equation is obtained as

$$Q(x) = \frac{Q_0V(L)}{L^2}\left[\mu_e\tau_e\left(1-\exp\left(-\frac{L(L-x)}{\mu_e\tau_eV(L)}\right)\right)\right.$$
$$\left. + \mu_h\tau_h\left(1-\exp\left(-\frac{xL}{\mu_h\tau_hV(L)}\right)\right)\right]. \quad (11)$$

When the electric field varies over x, Eq. (8) is used to solve $Q(x)$ numerically. A map of the charge collection efficiency, $CCE(x) \equiv Q(x)/Q_0$, can be generated to analyze the performance of a device.

2.2.2. Frisch collar detector

The physics and performance of the Frisch collar device has been thoroughly explained in the literature [32,31]. Fig. 2 shows the cross-section of a Frisch collar device. The conductive collar is either grounded or biased at a potential in between ground and the collecting contact's bias. The Frisch collar of the device used in this study was coupled to the grounded cathode. Therefore the analysis for the device reduces from a three terminal device to a two terminal device. Further, the device can be analyzed along its central line, hence, the analysis is reduced to 1D analysis as in the planar device configuration. Ramo's theorem can again be used to solve the induced current in the Frisch collar device. A numerical analysis method must be used to determine both the weighting field $E_w(x)$ and the actual electric field $E(x)$. Eq. (8) can be used to obtain $Q(x)$ due to the motion of charges along the central line of the device [31].

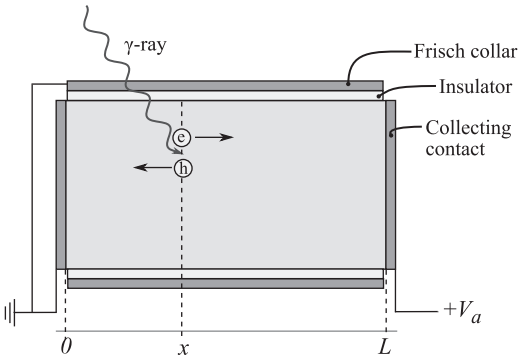

Fig. 2. Frisch collar device configuration.

3. Experimental procedure

3.1. Crystal growth

HgI_2 starting material was purified by sublimation in a dynamic vacuum, followed by melting, and finally with sublimation in static vacuum. After retrieval, the purified material was weighed and placed in a Pyrex ampoule 15 in. long and 41 mm in diameter. A low $\overline{M}_w$ polyethylene ($\overline{M}_w \sim 4000$ g/mol) was added to the ampoule and mixed directly with HgI_2. Approximately 80 g of HgI_2 and 1.6 g of low $\overline{M}_w$ polyethylene were used in the growth ampoule. The ampoule was sealed under vacuum ($\sim 10^{-4}$ Torr) and subsequently placed in a two-zone horizontal furnace. The source materials were positioned in the hot zone at 230 °C and the deposition zone was set at 150 °C.

Sublimated HgI_2 crystallizing at the end of the deposition zone was retrieved and placed in a new ampoule. The ampoule was sealed under vacuum as previously mentioned and was placed in a two-zone horizontal furnace. The source was positioned in the hot zone at 100 °C and the crystallization zone was set at 80 °C. The growth period was five days. At the end of the growth period the ampoule was retrieved and cooled down to room temperature by natural convective air.

HgI_2 grown with the low $\overline{M}_w$ polyethylene yields tetragonal prismatic crystals. These crystals typically appear as either single crystals or twinned crystals (Fig. 3). The most prominent crystal forms, (0 0 1) and {1 1 0}, are always found amongst the grown crystals. {h 0 1} planes of various size can be found as corner faces. The length of the crystals was observed to be parallel to the [0 0 1] axis.

3.2. HgI_2 planar device fabrication

As previously mentioned in Section 2.1, the (0 0 1) layers are held together by weak van der Waals bonds. Therefore, for device fabrication, a harvested crystal could be cut to the desired size with a razor blade. While sectioning the crystal, the aspect ratio was kept at a value between 1.5 and 2.0 [8]. Aquadag E was used as the contact material, applied to the crystal ends immediately after the crystal was sectioned. Palladium wires were attached to the contacts for electrical contact. Note that no etching was performed during the planar device fabrication. The tetragonal prismatic shape of the as-grown single crystals significantly help with the Frisch collar device fabrication. The fortuitous crystal

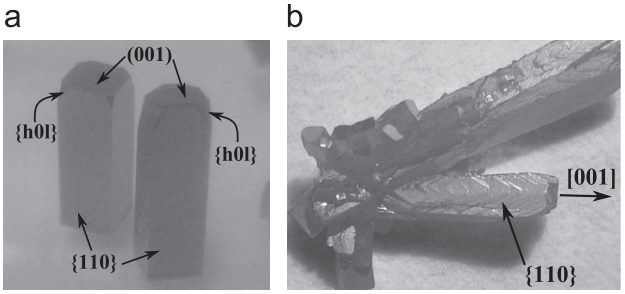

Fig. 3. Shown are (a) single and (b) twinned HgI_2 crystals grown with low $\overline{M}_w$ polyethylene. As can be seen the (0 0 1) and {1 1 0} faces are the most prominent faces, while {*h* 0 l} planes form the corner faces.

shape becomes more important for applications requiring numerous detectors (such as arrays).

3.3. HgI_2 Frisch collar device fabrication

Parylene-C was used as the first dielectric layer and it is commercially available in many variants [33]. In this study, Parylene-C was determined to be the best choice between the commercially available options because it is easy to use and has a fast deposition time. It also has a high resistivity ($8.8 \times 10^{10}\,\Omega\,cm$), a high dielectric breakdown strength (220 kV/mm), and a low dielectric constant ($\kappa \sim 2.95$) [34]. Parylene-C, which does not react with HgI_2, can be used to encapsulate the planar detector for passivation and stabilization. Parylene coating can also reinforce loose Aquadag contacts for additional mechanical support. This reinforcement allows for easy handling of the device.

Only a thin layer of Parylene-C was deposited as the first insulator layer on the surfaces of the HgI_2 planar device. The Parylene layer was kept very thin due to the fact that Parylene cannot be removed if the deposited layer is thick. Because there is always an optimum dielectric layer thickness for Frisch collar devices [35], other techniques, such as wrapping the device with Teflon tape, are recommended. Wrapping the Parylene coated device with Teflon allows for the optimum dielectric layer thickness for the HgI_2 planar device to be obtained. In this study, 37 mg of Parylene-C dimer was used, resulting in deposition of 50 μm Parylene-C as the first layer of dielectric material. This thin layer of Parylene-C was followed by two layers of 0.07 mm thick Teflon tape. Afterwards, a thin copper shim was cut to size and used as the Frisch collar, which extended the length of the device and was connected to the device cathode. In this manner, the Frisch collar was held at the cathode potential (both conductors were grounded) (Fig. 4).

3.4. Pulse height spectrum measurement

The fabricated HgI_2 detectors (planar and Frisch collar) were positioned in an aluminum test box for spectral collection of various radionuclides. The detector within the box was connected to an eV-550 preamplifier and both were placed inside a copper Faraday cage to minimize electronic noise. The measurement system consisted of an amplifier, an oscilloscope, a multi-channel analyzer (MCA), a high voltage supply, a pulse generator, and a personal computer, all positioned outside the Faraday cage. Gamma-ray sources (^{241}Am, ^{57}Co, ^{133}Ba, ^{137}Cs, ^{198}Au, and ^{60}Co) were always placed outside the aluminum test box, in the same position, such that the detector side faced the source.

During the experiment, the temperature and the relative humidity were recorded to be 21 °C and 75%, respectively. All operating parameters and settings were held constant for all

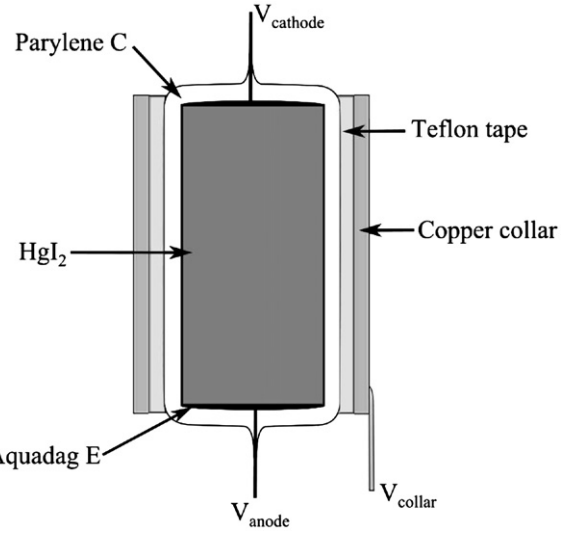

Fig. 4. HgI_2 Frisch collar detector cross-section.

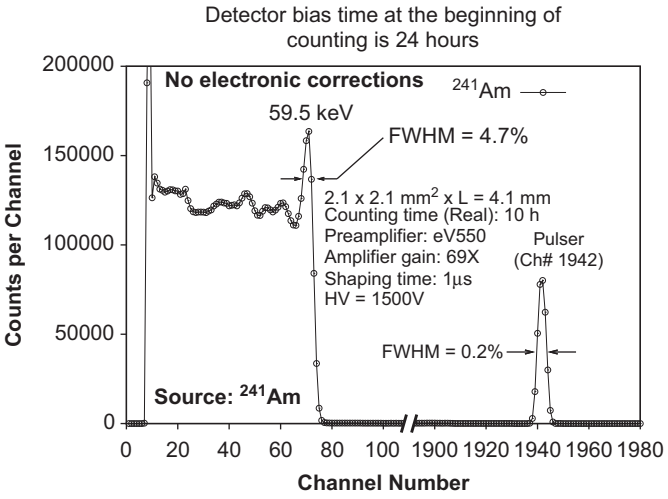

Fig. 5. Pulse height spectrum taken with a 2.1 × 2.1 × 4.1 mm^3 HgI_2 Frisch collar device being fully irradiated with a ^{241}Am gamma ray source positioned 3.0 cm away from the detector side. A 4.7% FWHM energy resolution is achieved at 59.5 keV.

measurements as follows. The amplifier shaping time was set to 1 μs and the amplifier gain was set to 69X. The detector was biased at +1500 V (applied to the anode) for more than 16 h (which is mentioned for each measurement) before taking the pulse-height spectra.

4. Results and discussion

For this study the pulse height spectra were collected from standard commercially available calibration sources of ^{241}Am, ^{57}Co, ^{133}Ba, ^{137}Cs, and ^{60}Co. A neutron activated ^{198}Au pulse height spectrum was also collected. The ^{198}Au source was activated by irradiating a 13 mg gold foil sample in the Kansas State University TRIGA Mk II nuclear reactor core for 8 min at 5 kW. The electronic settings were consistent for all measurements, and energy resolutions reported for gamma-ray full energy peaks are without any electronic corrections.

An energy resolution of 4.7% FWHM for the 59.5 keV spectral line of ^{241}Am was obtained, shown in Fig. 5. Shown in Fig. 6 is ^{57}Co spectrum where the energy resolution at the 122 keV is 4.0%

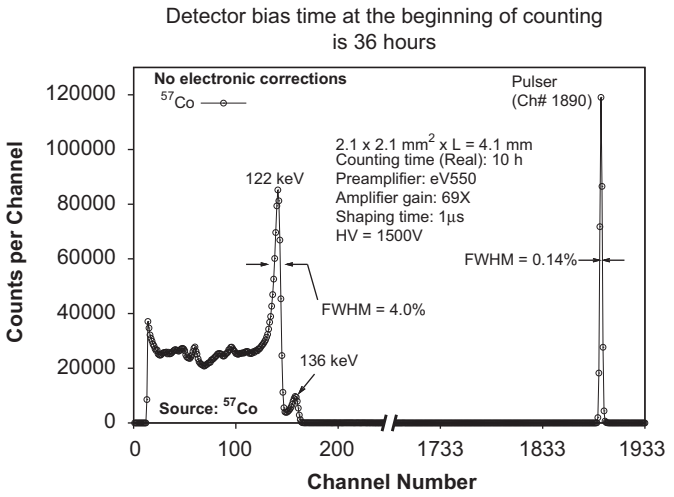

Fig. 6. Pulse height spectrum taken with a $2.1 \times 2.1 \times 4.1\,mm^3$ HgI_2 Frisch collar device being fully irradiated with a ^{57}Co gamma ray source positioned 3.0 cm away from the detector side. A 4.0% FWHM energy resolution is achieved at 122 keV.

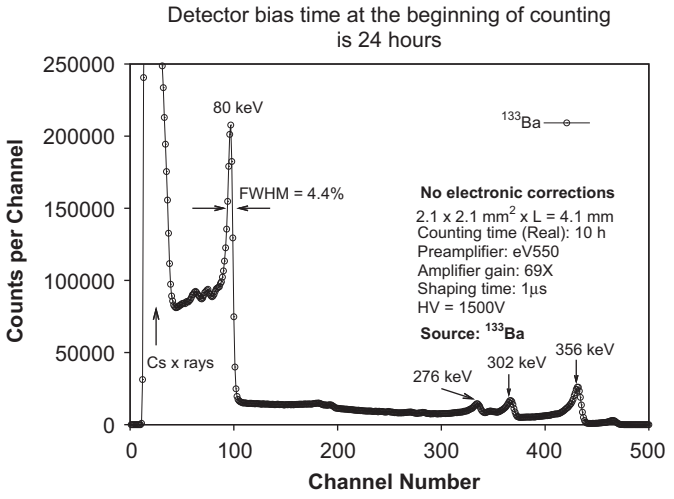

Fig. 7. Pulse height spectrum taken with a $2.1 \times 2.1 \times 4.1\,mm^3$ HgI_2 Frisch collar device being fully irradiated with a ^{133}Ba gamma ray source positioned 3.0 cm away from the detector side. A 4.4% FWHM energy resolution is achieved at 80 keV.

FWHM, and the 136 keV energy line is clearly observed. An energy resolution of 4.4% FWHM was achieved for the 80 keV spectral line of ^{133}Ba (see Fig. 7). The 356 keV photopeak of ^{133}Ba exhibited an energy resolution of 2.5% FWHM (see Fig. 8), with the 276, 302, and 382 keV emission energies of ^{133}Ba are also clearly observable.

The ^{198}Au spectrum is shown in Fig. 9 where the 411 keV full energy peak energy resolution is 2.6% FWHM. The 662 keV photopeak of ^{137}Cs with 1.8% FWHM energy resolution is also shown in Fig. 10. The Hg X-ray escape peaks are observable on both spectra of ^{198}Au and ^{137}Cs (Figs. 9 and 10). Fig. 11 displays the energy spectrum from ^{60}Co collected with the HgI_2 Frisch collar device. As shown, an energy resolution of 1.2% FWHM at 1173 keV energy line is achieved. Note that the relatively small HgI_2 device was capable of detecting the high energy gamma rays emitted from ^{60}Co.

The stability of the detector with time is also reported in Fig. 12, showing ^{137}Cs energy spectra over various irradiation times after initial operation. When the HgI_2 Frisch collar detector

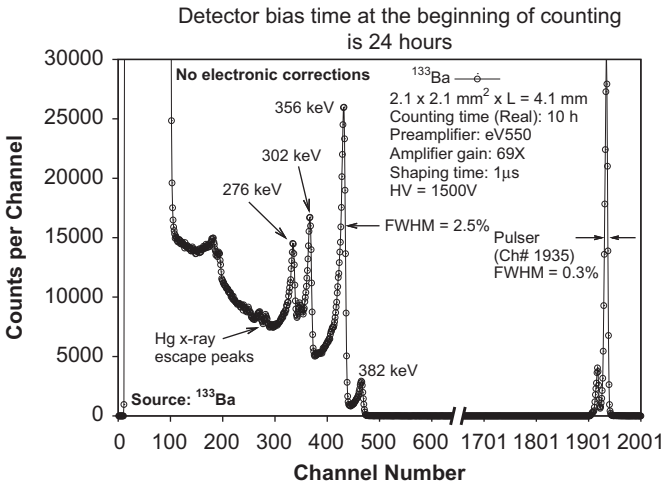

Fig. 8. Expanded view of the 276, 302, 356, and 382 keV full energy peaks of ^{133}Ba (see Fig. 7). A 2.5% FWHM energy resolution is achieved at 356 keV.

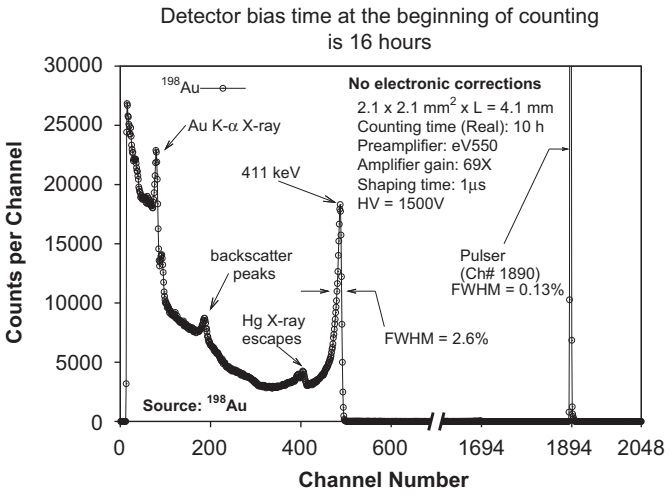

Fig. 9. Pulse height spectrum taken with a $2.1 \times 2.1 \times 4.1\,mm^3$ HgI_2 Frisch collar device being fully irradiated with a ^{198}Au gamma ray source positioned 3.0 cm away from the detector side. A 2.6% FWHM energy resolution is achieved at 411 keV.

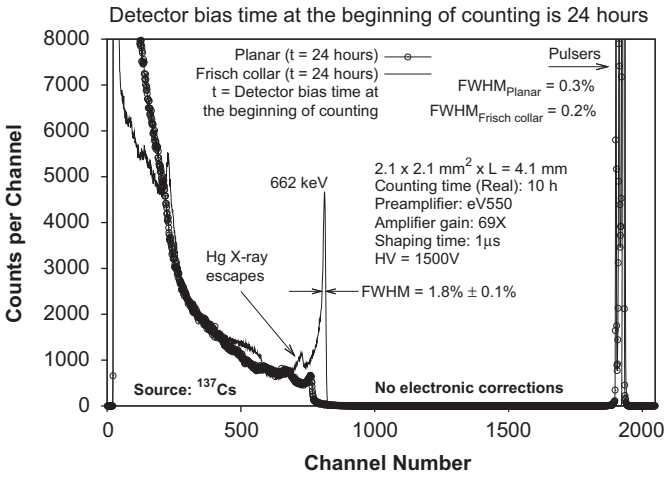

Fig. 10. Pulse height spectra taken with a $2.1 \times 2.1 \times 4.1\,mm^3$ HgI_2 device (Frisch collar and planar) being fully irradiated with a ^{137}Cs gamma ray source positioned 3.0 cm away from the detector side. A 1.8% FWHM energy resolution is achieved at 662 keV.

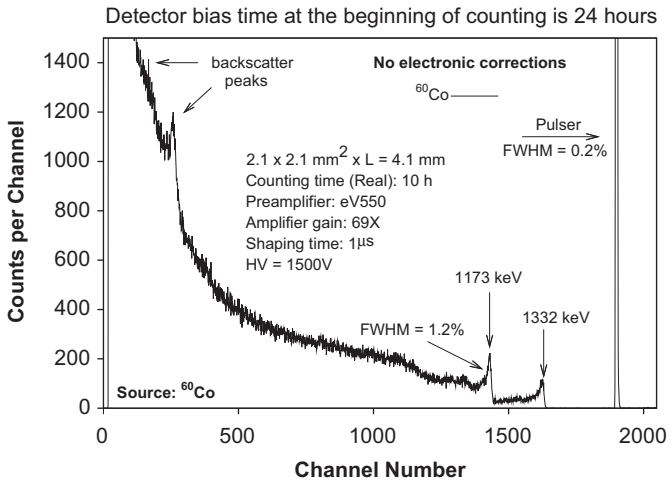

Fig. 11. Pulse height spectrum taken with a 2.1 × 2.1 × 4.1 mm^3 HgI_2 Frisch collar device being fully irradiated with a ^{60}Co gamma ray source positioned 3.0 cm away from the detector side. A 1.2% FWHM energy resolution is achieved at 1173 keV.

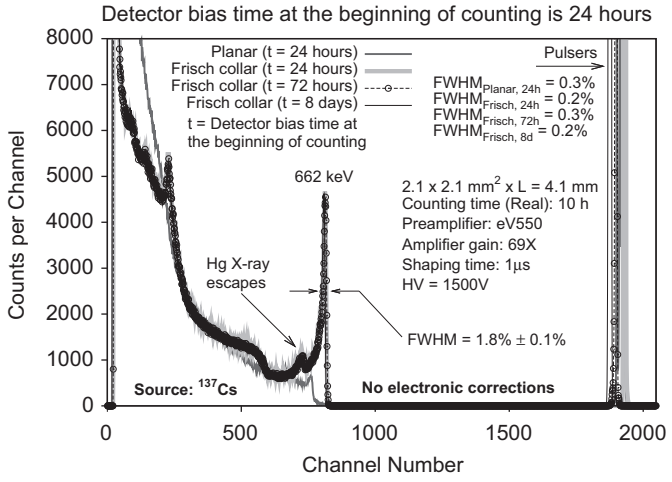

Fig. 12. Pulse height spectra taken with a 2.1 × 2.1 × 4.1 mm^3 HgI_2 device (Frisch collar and planar) being fully irradiated with a ^{137}Cs gamma ray source positioned 3.0 cm away from the detector side. A 1.8% FWHM energy resolution is achieved at 662 keV. The detector was under bias for different periods of time before each pulse height spectrum was collected.

had been under bias for more than 24 h, the pulse height spectrum remained more or else the same. In other words, the detector did not show polarization beyond 24 h of operation at high voltage.

5. Conclusions

HgI_2 growth with a low $\overline{M}_w$ polyethylene yields crystals with the fortuitous shape of tetragonal prisms, with the length of the crystals parallel to the [0 0 1] axis. For bar-shaped Frisch collar device fabrication, the aspect ratio of the crystals can be altered by simply cleaving crystal planes off the (0 0 1) face. No etching or polishing step was required in detector fabrication. Due to the application of the Frisch collar, no electronic correction or LN_2 cooling was needed to achieve excellent spectroscopic performance. The HgI_2 Frisch collar device performance, as seen in Fig. 12, did not change beyond 24 h of continuous bias application. Polarization was observed only up to about 10 h of continuous bias application. Studies on the polarization and de-polarization behaviors of the device are described elsewhere.

Acknowledgments

Funding is provided by the U.S. Department of Defense through Defense Threat Reduction Agency Basic Research contract HDTRA-01-07-1-007.

References

[1] G. Ottaviani, C. Canali, A.A. Quaranta, IEEE Trans. Nucl. Sci. NS-22 (1975) 192.
[2] G. Georgeson, F. Milstein, Nucl. Instr. and Meth. A 285 (1989) 488.
[3] V. Gerrish, Nucl. Instr. and Meth. A 322 (1992) 402.
[4] D. McGregor, R. Rojeski, High-resolution ionization detector and array of such detectors, US Patent No. 6,175,120, January 2001.
[5] W.J. McNeil, D.S. McGregor, A.E. Bolotnikov, G.W. Wright, R.B. James, Appl. Phys. Lett. 84 (2004) 1988.
[6] D.S. McGregor, A. Kargar, A.M. Jones, W.J. McNeil, M.J. Harrison, Nucl. Instr. and Meth. A 558 (2006) 497.
[7] A. Kargar, A.M. Jones, W.J. McNeil, M.J. Harrison, D.S. McGregor, Nucl. Instr. and Meth. A 558 (2) (2006) 497.
[8] A. Kargar, R.B. Lowell, M.J. Harrison, D.S. McGregor, The crystal geometry and the aspect ratio effects on spectral performance of CdZnTe Frisch collar device, in: Proceedings of the Society of Photo-Optical Instrumentation, vol. 6706, 2007, p. 67061J.
[9] I.F. Nicolau, J. Cryst. Growth 48 (1980) 51.
[10] I. Nicolau, J.P. Joly, J. Cryst. Growth 48 (1980) 61.
[11] M. Schieber, R. Carlston, H. Lamonds, P. Randtke, F. Schnepple, J. Llacer, Nucl. Instr. and Meth. 24–25 (1974) 205.
[12] M. Schieber, W. Schnepple, L. Van Den Berg, J. Cryst. Growth 33 (1976) 125.
[13] H. Lamonds, Nucl. Instr. and Meth. 213 (1983) 5.
[14] H. Scholz, Acta Electron. 17 (1974) 69.
[15] A.E. Bolotnikov, J. Baker, R. DeVito, J. Sandoval, L. Szurbart, IEEE Trans. Nucl. Sci. NS-52 (2005) 468.
[16] S. Faile, A. Dabrowski, G. Huth, J. Iwanczyk, J. Cryst. Growth 50 (3) (1980) 752.
[17] A. Burger, M. Roth, M. Schieber, J. Cryst. Growth 56 (1982) 526.
[18] A. Burger, A. Levi, J. Nissenbaum, M. Roth, M. Schieber, J. Cryst. Growth 72 (1985) 643.
[19] J. Laskowski, H. Kuc, K. Conder, J. Przyłuski, Mater. Res. Bull. 22 (6) (1987) 715.
[20] J. Przyłuski, J. Laskowski, Nucl. Instr. and Meth. A A283 (1989) 144.
[21] G.A. Jeffrey, M. Vlasse, Inorg. Chem. 6 (2) (1967) 396.
[22] M. Hostettler, H. Birkedal, D. Schwarzenbach, Chimia 55 (6) (2001) 541.
[23] T. Hahn, U. Shmueli, A.J.C. Wilson, I. U. of Crystallography, International Tables for Crystallography, D. Reidel Pub. Co., Dordrecht, Holland, 1984.
[24] J.D. Jackson, Classical Electrodynamics, John Wiley & Sons, Inc., 1999.
[25] W. Shockley, J. Appl. Phys. 9 (1938) 635.
[26] S. Ramo, IRE Proc. 27 (1939) 584.
[27] G. Cavalleri, G. Fabri, E. Gatti, V. Svelto, Nucl. Instr. and Meth. 21 (1963) 177.
[28] G. Cavalleri, G. Fabri, E. Gatti, V. Svelto, Nucl. Instr. and Meth. 92 (1971) 137.
[29] G.F. Knoll, D.S. McGregor, Fundamentals of semiconductor detectors for ionizing radiation, in: Materials Research Society Symposium Proceedings, vol. 302, 1993, pp. 3–17.
[30] V. Radeka, Ann. Rev. Nucl. Part. Sci. 38 (1988) 217.
[31] A. Kargar, A.C. Brooks, M.J. Harrison, D.S. McGregor, Characterization of charge collection in a CdZnTe Frisch collar detector with a highly collimated ^{137}Cs source, Nucl. Instr. Meth. A (2010), doi:10.1016/j.nima.2010.08.057.
[32] D. McGregor, R. Rojeski, IEEE Trans. Nucl. Sci. NS-46 (3 I) (1999) 250.
[33] Specialty coating systems, Model PDS 2010 LABCOTER 2 Operator's Manual, 2006.
[34] P.S. Ho, J. Leu, W.W. Lee, Low Dielectric Constant Materials for IC Applications, first ed., Springer, New York, 2003.
[35] A. Kargar, A.C. Brooks, M.J. Harrison, K.T. Kohman, R.B. Lowell, R.C. Keyes, H. Chen, G. Bindley, D.S. McGregor, IEEE Trans. Nucl. Sci. NS-56 (2009) 824.